Shotcrete: Elements of a System – Bernard (ed)
© 2010 Taylor & Francis Group, London, ISBN 978-0-415-47589-1

Crack widths in ASTM C-1550 panels

E.S. Bernard & G.G. Xu
TSE P/L, Penrith, Australia

ABSTRACT: Maximum permissible crack widths are an important issue for many Fibre Reinforced Shotcrete (FRS) tunnel linings due to the influence cracks have on post-crack strength, durability, and water ingress. The relationship between crack width and the deflection expected to occur in ground stabilized using a FRS lining is also of interest to geotechnical engineers. When performance assessment tests are undertaken on FRS samples it is therefore necessary to evaluate performance at relevant crack widths. Given the widespread use of ASTM C1550 panels for post-crack performance assessment of FRS the relationship between the central deflection measured in this test and the corresponding maximum widths of the three radial cracks that normally form is of significance. A closed-form solution is presented for the angles of rotation and corresponding maximum crack widths in the three radial cracks that form in a C1550 test based on their orientation relative to the mid-point bisectors between the supports. The effect of the characteristic probability distribution in crack locations on variations in crack width and the magnitude of the average crack width is also considered.

1 INTRODUCTION

Many aspects of the in-service performance of Fibre Reinforced Shotcrete (FRS) are related to crack widths. The most notable of these include the relation between crack width and residual strength (Banthia & Trottier, 1994), deflection, durability of the concrete matrix (Neville, 1995), and susceptibility of fibres within the concrete to corrosion (Kosa & Naaman, 1990; Nordström, 2001). In post-crack performance assessment tests for FRS based on beams and panels the maximum crack width experienced by the specimen is controlled by the geometry of the specimen and the angle of rotation exhibited at the hinges that form after cracking of the concrete matrix. In the ASTM C1550 round panel test (ASTM, 2008) the magnitude θ_i of the Crack Rotation Angles (CRAs) that arise at the three radial cracks are influenced by the locations of the cracks relative to the mid-point bisectors between the adjacent pairs of pivoted supports and the deflection imposed at the centre (Figure 1).

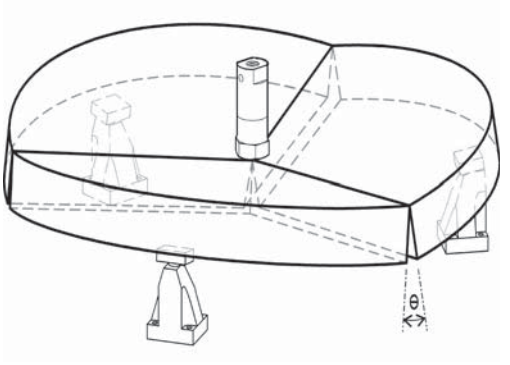

Figure 1. ASTM C1550 round panel test.

General characteristics of the failure modes in C1550 panels are described geometrically in Figure 2 for the case of three symmetrically occurring radial cracks and in Figure 3 for the general case of three radial cracks. Bernard & Xu (2008) recently presented an exact rigid plate analysis to determine the relation between crack location and the three CRAs. An approximate closed-form solution to this same problem is presented below together with comparisons to the exact solution and a discussion concerning the magnitude of errors associated with the rigid plate approximation to structural behaviour in the uncracked portions of a C1550 panel.

In the C1550 test the position of each supporting pivot remains fixed for all specimens but the locations of the three radial cracks that form are uncontrolled. The position of each crack is characterized by a Mid-point Offset Angle (MOA) relative to the corresponding mid-point bisector, namely, angles α, β, and γ (Figure 3). Tran et al. (2005) used measurements of crack locations in about five hundred C1550 panels to find that the distribution of Midpoint Offset Angles can be described very well by the Weibull probability density function (PDF), viz.

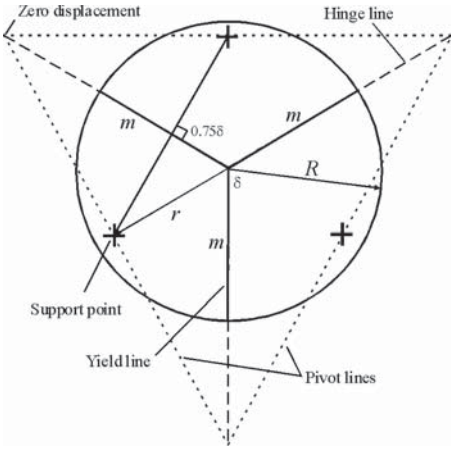

Figure 2. Folding plate analysis of ASTM C1550 panel with three symmetric radial cracks.

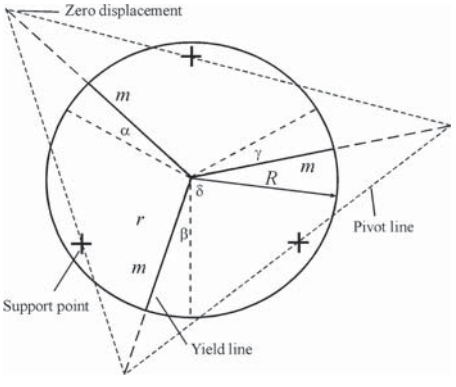

Figure 3. Folding plate Analysis of ASTM C1550 panel with three general radial cracks.

$$f(\alpha,\beta,\gamma) = \alpha_1\beta_1^{-\alpha_1}\gamma^{\alpha_1-1}e^{-(\gamma/\beta_1)^{\alpha_1}} \quad (1)$$

where $\alpha_1 = 1.108$ and $\beta_1 = 13.038°$. This PDF has presently been employed to conduct a Monte Carlo Simulation (MCS) to determine the characteristic distribution of the CRAs θ_α, θ_β and θ_γ for a sample population of C1550 panels. The CRAs were determined using both the exact analysis described by Bernard & Xu (2008) and the approximate closed-form method described in the Appendix. Random number generators were used together with the Weibull PDF to choose the sign and magnitude of α, β and γ, each of which were assumed to be independent. The summation $(\theta_\alpha + \theta_\beta + \theta_\gamma)$ produced as output from the MCS using the approximate closed-form solution was then assessed using Maximum Likelihood Estimation (Law & Kelton, 2000) and the Chi-square test (Kendall & Stuart, 1979) to determine which of three probability distributions (the Gaussian, Weibull, and Lognormal functions; Johnson et al., 1994) best described the outcome. The CRAs θ_α, θ_β and θ_γ were then used to estimate crack widths in the panels.

2 RESULTS

Using the Monte Carlo Simulation technique referred to above, the variation in $(\theta_\alpha + \theta_\beta + \theta_\gamma)$ with $(\alpha + \beta + \gamma)$ for a unit central deflection δ was found to be described by the distribution shown in Figure 4 (all angles in degrees). The quantity $(\theta_\alpha + \theta_\beta + \theta_\gamma)$ displayed a minimum equal to $3\sqrt{3}\delta_0 / r = 0.794$ degrees for the symmetric pattern of radial cracks. This value is derived from a geometric analysis of the angle at each radial hinge that arises when a deflection δ is imposed at the centre (Tran et al., 2001).

As $(\alpha + \beta + \gamma)$ departed from zero, the quantity $(\theta_\alpha + \theta_\beta + \theta_\gamma)$ increased in magnitude. As $|\alpha| + |\beta| + |\gamma|$ departed from zero, $(\theta_\alpha + \theta_\beta + \theta_\gamma)$ also increased in magnitude (see Figure 5, all angles in degrees). However, $(\theta_\alpha + \theta_\beta + \theta_\gamma)$ appeared to be relatively insensitive to the magnitude of each MOA. When $|\alpha| + |\beta| + |\gamma| = 60°$ we find that $(\theta_\alpha + \theta_\beta + \theta_\gamma)$ is, on average, 11% greater than the minimum obtained for the symmetric case, and for $|\alpha| + |\beta| + |\gamma| = 100°$ we find that $(\theta_\alpha + \theta_\beta + \theta_\gamma)$ is, on average, 37% greater. This indicates that the approximate solution is less sensitive to the midpoint angles than the exact solution which indicated a 55% difference at $|\alpha| + |\beta| + |\gamma| = 100°$ (Bernard & Xu, 2008). It must be noted, however, that based on the distribution represented by Equation (1), the likelihood that $|\alpha| + |\beta| + |\gamma| \geq 100°$ is less than 0.01 percent.

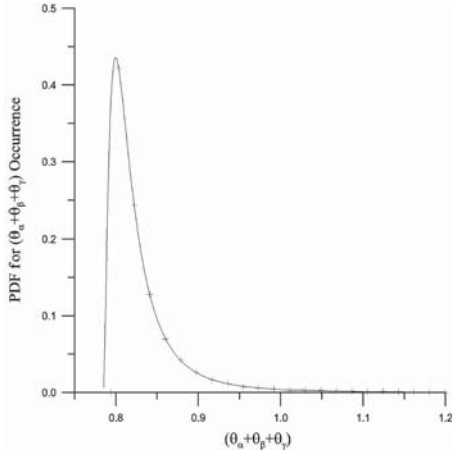

Figure 4. Occurrence frequency for $(\theta_\alpha + \theta_\beta + \theta_\gamma)$.

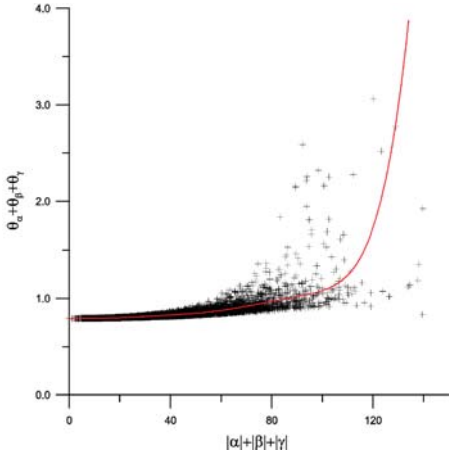

Figure 5. Magnitude of $(\theta_\alpha + \theta_\beta + \theta_\gamma)$ as a function of the sum of the midpoint angles.

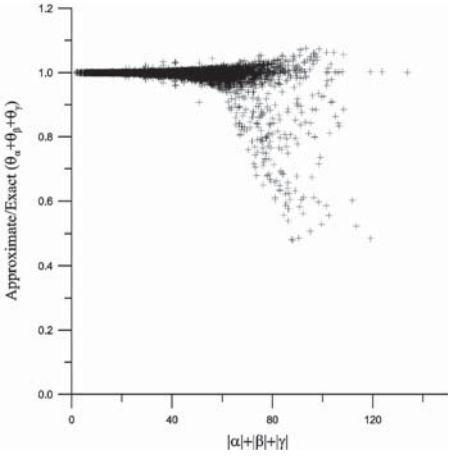

Figure 6. Ratio of approximate $(\theta_\alpha + \theta_\beta + \theta_\gamma)$ over exact values as a function of the sum of midpoint angles.

When the characteristic distribution of $(\theta_\alpha + \theta_\beta + \theta_\gamma)$ obtained by the MCS was assessed using the method of Maximum Likelihood Estimation to determine the best fitting Probability Distribution Function (PDF) the distribution was assessed for a simulated sample of specimens represented by Equation (1) (Figure 4). It was found that the three-parameter Lognormal distribution was the most suitable for describing the quantity $(\theta_\alpha + \theta_\beta + \theta_\gamma)$ since using this distribution achieved the maximum likelihood. The lognormal distribution gave a mean of 0.837 degrees, a standard deviation (SD) of 0.063 degrees, and a COV of 7.54% for $(\theta_\alpha + \theta_\beta + \theta_\gamma)$. The mean was therefore only 5.4% greater than the minimum associated with the symmetric cracking case. Moreover, the average for the approximate analysis was only 0.1% greater than for the exact analysis. This suggests that characteristic variations in crack location have, on average, a small influence on the sum of the CRAs experienced at the cracks compared to the symmetric case. Examination of Figure 5 and comparison with the results by Bernard & Xu (2008) for the exact case suggests that the magnitude of the variation in angles between the exact and approximate methods differs by a negligible amount for $|\alpha| + |\beta| + |\gamma| \leq 60°$ (Figure 6). The difference becomes more significant when the cracks occur closer to the pivoted supports.

The Monte Carlo Simulation was conducted using estimates of Crack Rotation Angles obtained by the approximate method (see the Appendix) for a progressively increasing central deflection. The results indicated that the magnitude of the mean CRAs obtained using the approximate closed-form solution were greater than for the exact analysis presented by Bernard & Xu (2008), especially as

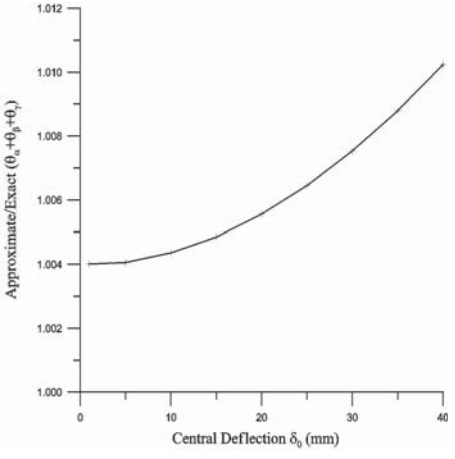

Figure 7. Ratio of approximate $(\theta_\alpha + \theta_\beta + \theta_\chi)$ over exact values as a function of central deflection for a characteristic distribution of α, β, and γ. Each point represents the mean of a distribution of ratios at each given deflection.

the central deflection approached 40 mm, but the maximum mean error was nevertheless no greater than 1% (Figure 7). This error was due in part to the simplification $\theta_i \cong \sin\theta_i$ that was incorporated into the approximate method since $\theta_i \geq \sin\theta_i$ for large θ_i and $\theta_i \cong \sin\theta_i$ only for very small θ_i. The mean magnitude of $(\theta_\alpha + \theta_\beta + \theta_\gamma)$ obtained by the approximate method was 0.4% greater than that obtained using the exact solution when the central deflection $\delta = 0$ because of the cumulative effect of $\theta_i \cong \sin\theta_i$ on each of the crack angles given the characteristic variation in α, β, and γ used in obtaining this estimate.

The approximate method of analysis served to demonstrate that the exact method was free from

gross errors. Both methods predicted a relationship between MOAs and CRAs broadly similar to that described by Holmgren & Norlin (2001).

3 DISCUSSION

3.1 *Relationship between crack rotation angle and crack width*

The analyses described above generated estimates of Crack Rotation Angles (CRAs) in each radial crack in a C1550 panel. In order to obtain estimates of the corresponding maximum crack widths it is necessary to select a relation between these two parameters. Since the analysis above was based on a rigid plate model of panel behaviour, it is consistent to also use a model incorporating rigid rotating plates at each hinge in which case the maximum crack width w at each hinge is simply related to the panel thickness t by the expression.

$$w = \theta t \tag{2}$$

This model assumes that each adjacent pair of panel sectors rotate about a line at the upper surface at which they meet. This model is quite satisfactory for plain concrete panels and quite possibly very lightly reinforced panels as well. However, most FRS displays a degree of post-crack residual strength that is manifested as a flexural-tensile stress distribution varying in magnitude through the lower portion of the C1550 panel. The tensile stresses are balanced by compressive stresses in the upper regions. There exists a neutral axis of zero stress at some depth from the upper surface which represents the point about which crack rotations should be calculated. Unfortunately, the indeterminate nature of the distribution of stress through a panel, plus the fact that membrane action causes a net tensile stress to act near the centre of the panel and net compressive stress to occur near the edges, means that it is very difficult to estimate the location of the neutral axis. Based on estimates of the rigidity of FRS before and after cracking (Bernard, 2008), the neutral axis is unlikely to be located further than $t/10$ from the upper surface, and thus the maximum crack width for most FRS will lie somewhere in the range $0.9\theta t < w < \theta t$.

Using the approximations presented above the distribution of crack widths occurring in C1550 panels can be found as a simple multiple of the distributions of CRAs developed in Section 2. The exact estimate of the crack width w in each radial crack for the symmetric cracking case (Figure 2) based on a rigid plate model is found as

$$w = \frac{\sqrt{3}\delta t}{r} \tag{3}$$

where r is the radius to the pivoted supports. Taking into account the distribution of MOAs (Eq. 1), which tends to increase the average crack width, and assuming an average neutral axis depth of $t/20$, a more realistic estimate of average maximum crack width in C1550 panels is

$$w = 0.95 \times 1.05 \times \frac{\sqrt{3}\delta t}{r} = \frac{1.73\delta t}{r} \tag{4}$$

3.2 *Errors due to the rigid plate approximation*

The analyses described above were all undertaken using a rigid plate model to estimate the magnitude of post-crack rotation angles in C1550 panels. This model ignores the fact that real panels suffer quasi-elastic deformation of the uncracked sectors when under load. A means of estimating the error in the CRAs due to the rigid plate approximation is therefore presented below.

Prior to cracking the CRAs are obviously zero, hence estimation of errors in the CRAs must commence at the point of cracking in the load-deflection curve. After initiation of the three radial cracks and attainment of the associated first peak in load resistance most FRC exhibits strain-softening behaviour, thus the maximum curvature experienced in the uncracked sectors of the panel will occur when the cracks are initiated. The fall in load resistance that usually occurs after cracking leads to elastic relaxation within the uncracked sectors and a reduction in associated curvature. The result is that the true CRAs at the three radial cracks will be smaller than suggested by the rigid plate model.

Laboratory measurements and elastic numerical modelling of structural behaviour (Figure 8, see also Bernard & Pircher, 2001) indicate that the deflection at the center of a C1550 panel in response to a point load is about 0.5 mm at the point of first cracking of the concrete matrix. Depending on the strength, age, and composition of the FRC, the stiffness at the center varies in the range 50–70 kN/mm. The total post-crack rotation θ_T experienced at one of the radial cracks can be approximated as

$$\theta_T = \theta_{RP} - \theta_e \tag{5}$$

where θ_{RP} is the rotation predicted by the rigid plate model and θ_e is the rotation due to quasi-elastic relaxation of the adjacent uncracked sectors. The magnitude of θ_e can be estimated by calculating the rigid plate rotation equivalent to a post-crack central deflection of 0.5 mm and scaling this in proportion to the fall in post-crack load resistance of the panel $P_{cr} - P_r$ divided by the load resistance at cracking P_{cr}, viz.

$$\theta_e = \frac{P_{cr} - P_r}{P_{cr}} \theta_{0.5} \tag{6}$$

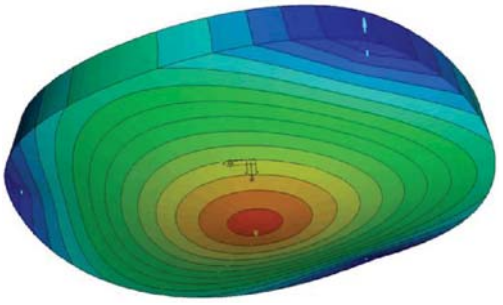

Figure 8. Distribution of normalized deflections on underside of a C1550 panel in response to a central point load.

The magnitude of $\theta_{0.5}$ is approximately equal to the rotation experienced at a post-crack central deflection of 0.5 mm for a FRC panel exhibiting no residual load resistance. This rotation has been taken to be modelled satisfactorily using the rigid plate approximation.

For a strain-softening FRC, errors in the CRAs due to the rigid plate approximation will be most significant immediately after cracking, but as the central deflection increases and the residual load resistance falls the relative magnitude of the errors become smaller. The significance of the error can be found by calculating the magnitude of θ_T and comparing this to θ_{RP} for a characteristic distribution of MOAs. The magnitude of error associated with the rigid plate approximation has been estimated for several load-deflection responses (Figure 9). These models represent successively more brittle FRC with a bi-linear fall in residual capacity immediately after cracking ranging from 99 to 25 percent of the peak load resistance. The results, shown in Figure 10, confirm that the errors in CRAs due to the rigid plate approximation are more significant the tougher the FRC is and the smaller the central deflection is. If the average post-crack capacity of commercial FRS is taken to be about 50% of peak load resistance at cracking, errors in the CRAs due to the rigid plate approximation will be no more than 1% for a deflection of about 5 mm or 5% for a deflection of 1 mm. For lightly reinforced FRC with a post-crack residual load capacity less than 25% of the peak the rigid plate approximation is sufficiently accurate at all deflections.

Note that the present geometric analysis based on rigid folding plates ignores the fact that the panel suffers membrane tension around the centre instead of pure flexure. The maximum crack widths experienced by a C1550 panel beyond ~20 mm central deflection are therefore somewhat greater than indicated by the analysis presented above.

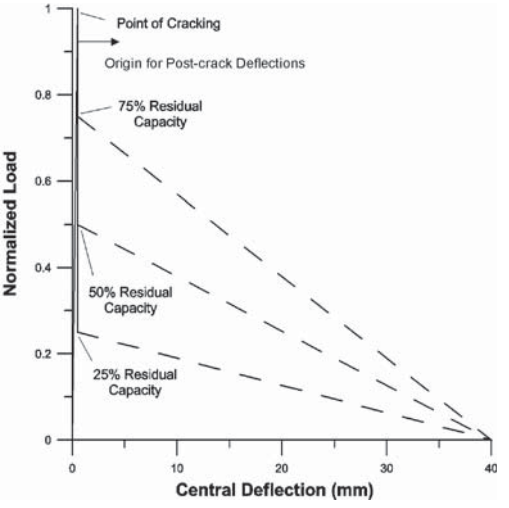

Figure 9. Simplified specimen behaviours used to assess magnitude of errors associated with the rigid plate approximation.

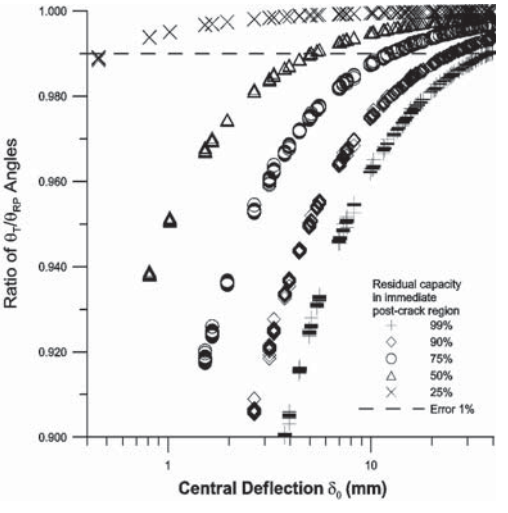

Figure 10. Magnitude of errors in average CRA involved in use of rigid plate approximation for models shown in Figure 9.

4 CONCLUSIONS

In this investigation an approximate closed-form solution for the angles of rotation in the three radial cracks that form in a C1550 panel was presented. This model predicts angles that are slightly larger than predicted using an exact rigid plate analysis developed elsewhere. Both models estimate average crack widths that are larger than predicted on the basis of the symmetric pattern of radial cracks

because average crack widths increase as the location of each crack approaches the pivoted supports in this test.

The rigid plate model was found to over-estimate crack widths compared to actual FRS panels that exhibit post-crack residual strength because of curvature in the uncracked portions of the panel and the fact that the neutral axis is typically not located at the upper surface of the specimen. However, membrane effects at larger deflections lead to a non-uniform distribution of crack width along each radial crack. At large deflections crack widths are wider near the centre and narrower near the edge of the specimen than is predicted by the rigid plate model.

REFERENCES

ASTM International, Standard C1550. "Standard Test Method for Flexural Toughness of Fiber Reinforced Concrete (Using Centrally Loaded Round Panel)", ASTM, West Conshohocken, 2008.

Banthia, N. & Trottier, J.-F., 1994. "Concrete Reinforced with Deformed Steel Fibers, Part 1: Bond-Slip Mechanisms", *ACI Materials Journal*, Vol. 91, No. 5, Sept-Oct, pp. 435–446.

Bernard, E.S., 2008. "Post-Crack Flexural Modulus of Fibre-Reinforced Shotcrete", *Fifth International Symposium on Sprayed Concrete*, pp. 48–59. Lillehammar, Norway, April 21–24.

Bernard, E.S. & Pircher, M., 2001. "The Influence of Thickness on Performance of Fiber-Reinforced Concrete in a Round Determinate Panel Test", *Cement, Concrete, and Aggregates*, CCAGDP, Vol. 23, No. 1, pp. 27–33.

Bernard, E.S. & Xu, G.G., 2008. "The Effect of Radial Crack Locations on Load Resistance of C1550 Panels", *Journal of ASTM International*, Vol. 5, No. 10, Paper ID JAI01739.

Holmgren, J. & Norlin, B., 2001 "Properties and the use of the round determinately supported concrete panel for testing of fibre reinforced concrete", Workshop on *The Design of Steel Fibre Reinforced Concrete Structures*, Stockholm, June 12, The Nordic Concrete Federation.

Johnson, N.L., Kotz, S. & Balakrishnan, N., 1994. *Continuous Univariate Distributions*, Vol. 1, 2nd Ed., John Wiley & Sons, New York.

Kendall, M. & Stuart, A., 1979. *The Advanced Theory of Statistics, Volume 2: Inference and Relationship*, 4th Ed., Charles Griffin & Co., England.

Kosa, K. & Naaman, A.E., 1990. "Corrosion of Steel Fiber Reinforced Concrete", *ACI Materials*, Vol. 87, No. 1, Jan-Feb, pp. 27–37.

Law, A.M. & Kelton, W.D., 2000. *Simulation Modelling and Analysis*, 3rd Ed., McGraw-Hill, New York.

Neville, A.M., 1995. *Properties of Concrete*, 4th Ed., Longman.

Nordström, E., 2001. "Durability of Steel Fibre Reinforced Shotcrete with Regard to Corrosion", *Shotcrete: Engineering Developments*, Bernard (ed.), pp. 213–217, Swets & Zeitlinger, Lisse.

Tran, V.G., Beasley, A.J. & Bernard, E.S., 2001. "The Application of Yield Line Theory to Round Determinate Panels", *Shotcrete: Engineering Developments*, Bernard (ed.), pp. 245–254, Swets & Zeitlinger, Lisse, 2001.

Tran, V.N.G., Bernard, E.S., & Beasley, A.J., 2005. "Constitutive Modelling of Fiber Reinforced Shotcrete Panels", *Journal of Engineering Mechanics*, ASCE, Vol. 131, No. 5, May, pp. 512–521.

APPENDIX—APPROXIMATE DETERMINATION OF CRACK ROTATION ANGLES USING STRAIN COMPATIBILITY

For the purposes of the present analysis of a C1550 panel, the three sectors occurring between the radial cracks have been taken to be rigid plates, deflections are assumed to be small, and membrane tension is ignored. The model of the panel used for this analysis is shown in Figure A1. The three pivots are symmetrically arranged at the points 1, 2 and 3. The points A, B and C occur at the intersection between each radial crack and the edge of the panel. δ_α, δ_β, δ_γ and δ_o are the deflections at the points A, B, C and the panel center O. The three midpoint offset angles (MOAs) α, β and γ define the location of the three radial cracks relative to the midpoints bisecting each sector and are measured clockwise positive. The rotations at the three radial cracks corresponding at these offset angles are θ_α, θ_β, and θ_γ. The radius of the panel is R and the radius to the supports is r. In this analysis it is assumed that $\theta_i \cong \sin\theta_i$, hence errors will arise as deflections increase.

A1.1 *Determination of deflections at edge of panel*

The angle of crack rotation at each of the three radial cracks can be found by first calculating the deflections at the points where the radial cracks intersect the edge of the panel. Each of these deflections is found by a process based on rotation of the rigid plates on either side of each crack and the fact that the deflection at the supporting pivots is zero. The maximum deflection suffered by the panel is δ_0 at the centre. Taking a normal from one radial crack to each of the adjacent pivots (Figure A1), we have

$$x_1 = r\cos(\pi/3 + \beta) \quad \text{and} \quad x_2 = r\cos(\pi/3 - \beta) \tag{A1}$$

$$h_1 = r\sin(\pi/3 + \beta) \quad \text{and} \quad h_2 = r\sin(\pi/3 - \beta) \tag{A2}$$

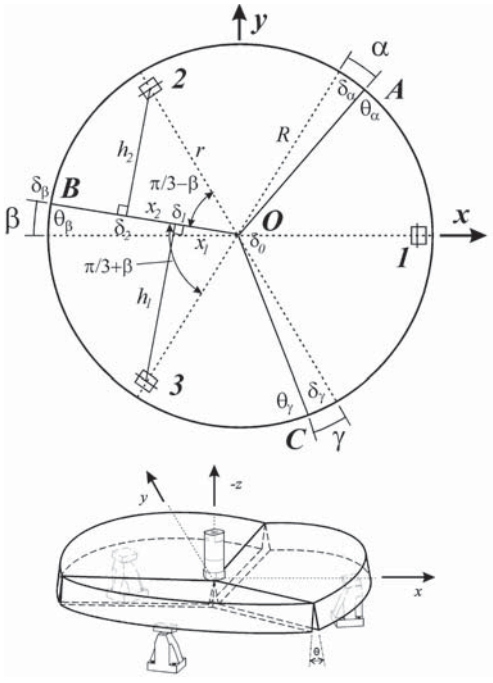

Figure A1. General cracking pattern for a C1550 panel and axis directions.

The deflections at the intersections between the normal from each pivot and the crack are

$$\delta_1 = \delta_0 + \frac{x_1}{R}(\delta_\beta - \delta_0) \quad \text{and} \quad \delta_2 = \delta_0 + \frac{x_2}{R}(\delta_\beta - \delta_0) \tag{A3}$$

Given that the two sectors on each side of the crack are rigid plates, we have $\theta_\beta = \theta_1 + \theta_2$, thus

$$\theta_1 = \frac{\delta_1}{h_1} = \left[\delta_0 + \frac{r\cos(\pi/3+\beta)}{R}(\delta_\beta - \delta_0)\right] \Big/ r\sin(\pi/3+ \tag{A4}$$

$$\theta_2 = \frac{\delta_2}{h_2} = \left[\delta_0 + \frac{r\cos(\pi/3-\beta)}{R}(\delta_\beta - \delta_0)\right] \Big/ r\sin(\pi/3- \tag{A5}$$

$$\theta_1 + \theta_2 = \left[\delta_0 + \frac{r\cos(\pi/3+\beta)}{R}(\delta_\beta - \delta_0)\right] \Big/ r\sin(\pi/3+\beta) + \left[\delta_0 + \frac{r\cos(\pi/3-\beta)}{R}(\delta_\beta - \delta_0)\right] \Big/ r\sin(\pi/3-\beta)$$

Collecting terms, we find for the deflection at β

$$\theta_\beta = \frac{\delta_0 \sin(\pi/3-\beta) + r\cos(\pi/3+\beta)\sin(\pi/3-\beta)(\delta_\beta - \delta_0)/R}{r\sin(\pi/3+\beta)\sin(\pi/3-\beta)} + \frac{\delta_0 \sin(\pi/3+\beta) + r\cos(\pi/3-\beta)\sin(\pi/3+\beta)(\delta_\beta - \delta_0)/R}{r\sin(\pi/3+\beta)\sin(\pi/3-\beta)} \tag{A6}$$

The compound terms can be simplified using $\sin(\pi/3+\beta)\sin(\pi/3-\beta) = 2\cos 2\beta + 1$, $\sin(\pi/3+\beta) + \sin(\pi/3-\beta) = \sqrt{3}\cos\beta$, and $\cos(\pi/3+\beta)\sin(\pi/3-\beta) + \cos(\pi/3-\beta)\sin(\pi/3+\beta) = \frac{\sqrt{3}}{2}$

thus

$$\theta_\beta(1+2\cos 2\beta)\frac{R}{2\sqrt{3}} = \delta_0\left[\frac{2R}{r}\cos\beta - 1\right] + \delta_\beta \tag{A7}$$

similarly

$$\theta_\alpha(1+2\cos 2\alpha)\frac{R}{2\sqrt{3}} = \delta_0\left[\frac{2R}{r}\cos\alpha - 1\right] + \delta_\alpha \tag{A8}$$

and

$$\theta_\gamma(1+2\cos 2\gamma)\frac{R}{2\sqrt{3}} = \delta_0\left[\frac{2R}{r}\cos\gamma - 1\right] + \delta_\gamma \tag{A9}$$

The relationship between the deflection at the extremity of each radial crack δ_i and the deflection in the adjacent cracks can be found using strain compatibility (Figure A2). Each sector between pairs of radial cracks experiences rigid body motion, hence the rotation about a line joining the pivot and the centre of the panel can be used to equate rotations associated with the deflections at the extremities of the panel.

Taking a normal from each crack to the line joining the pivot and the centre of the panel, we have

$x_3 = R\cos(\pi/3 - \beta)$ and $x_4 = R\cos(\pi/3 + \alpha)$

$h_3 = R\sin(\pi/3 - \beta)$ and $h_4 = R\sin(\pi/3 + \alpha)$

The deflection at the centre is δ_0 and the deflection at the pivot is zero. Hence, the deflection at the intersection between the normal from each crack (Figure A2) and the pivot line is found as

$$\delta_3 = \delta_0\left[1 - \frac{R}{r}\cos(\pi/3-\beta)\right] \quad \text{and} \quad \delta_4 = \delta_0\left[1 - \frac{R}{r}\cos(\pi/3+\alpha)\right]$$

$$\theta_3 = \frac{(\delta_\beta - \delta_3)}{h_3} = \left[\delta_\beta - \delta_0\left[1 - \frac{R\cos(\pi/3-\beta)}{r}\right]\right] \Big/ R\sin(\pi/3-\beta)$$

$$\theta_4 = \frac{(\delta_4 - \delta_\beta)}{h_4} = \left[\delta_0\left[1 - \frac{R\cos(\pi/3+\alpha)}{r}\right] - \delta_\beta\right] \Big/ R\sin(\pi/3+\alpha) \tag{A10}$$

Now $\theta_3 = \theta_4$, so

$$\delta_\alpha - \delta_0\left[1 - \frac{R}{r}\cos(\pi/3-\beta)\right] = \left[\delta_0\left[1 - \frac{R}{r}\cos(\pi/3+\alpha)\right] - \delta_\beta\right] \times \frac{\sin(\pi/3-\beta)}{\sin(\pi/3+\alpha)} \tag{A11}$$

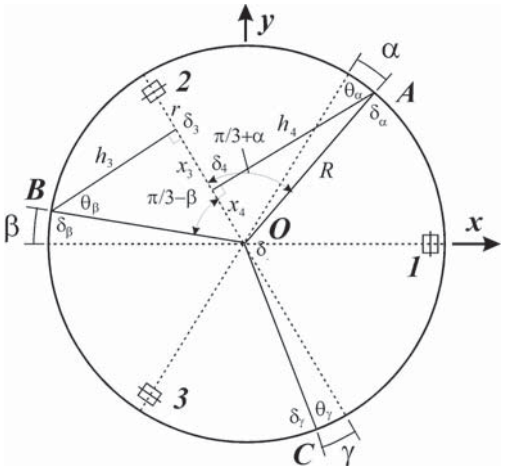

Figure A2. The effect of offset angles α and β on the deflections δ_α and δ_β in adjacent cracks.

Re-arranging terms, we find

$$\delta_\alpha + \delta_\beta\left[\frac{\sin(\pi/3-\beta)}{\sin(\pi/3+\alpha)}\right] = \delta_0\left[1+\frac{\sin(\pi/3-\beta)}{\sin(\pi/3+\alpha)} - \frac{R}{r} \times\left[\frac{\sin(2\pi/3+\alpha-\beta)}{\sin(\pi/3+\alpha)}\right]\right] \quad \text{(A12)}$$

Similarly,

$$\delta_\beta + \delta_\gamma\left[\frac{\sin(\pi/3-\gamma)}{\sin(\pi/3+\beta)}\right] = \delta_0\left[1+\frac{\sin(\pi/3-\gamma)}{\sin(\pi/3+\beta)} - \frac{R}{r} \times\left[\frac{\sin(2\pi/3+\beta-\gamma)}{\sin(\pi/3+\beta)}\right]\right] \quad \text{(A13)}$$

and

$$\delta_\gamma + \delta_\alpha\left[\frac{\sin(\pi/3-\alpha)}{\sin(\pi/3+\gamma)}\right] = \delta_0\left[1+\frac{\sin(\pi/3-\alpha)}{\sin(\pi/3+\gamma)} - \frac{R}{r} \times\left[\frac{\sin(2\pi/3+\gamma-\alpha)}{\sin(\pi/3+\gamma)}\right]\right] \quad \text{(A14)}$$

A1.2 *Solution of equations*

The expressions listed above relating the deflection at the extremity of each radial crack represent three independent equations with three unknown deflections. This system of equations can be solved using

$$a\delta_\alpha + \delta_\gamma = \delta_0 e$$
$$\delta_\alpha + b\delta_\beta = \delta_0 f \quad \text{or}$$
$$\delta_\beta + c\delta_\gamma = \delta_0 g$$

$$\begin{bmatrix} a & 0 & 1 \\ 1 & b & 0 \\ 0 & 1 & c \end{bmatrix}\begin{Bmatrix} \delta_\alpha \\ \delta_\beta \\ \delta_\gamma \end{Bmatrix} = \delta_0\begin{Bmatrix} e \\ f \\ g \end{Bmatrix} \quad \text{(A15)}$$

which can be represented as

$$\boldsymbol{A}x = \boldsymbol{d}$$

where

$$a = \frac{\sin(\pi/3-\alpha)}{\sin(\pi/3+\gamma)} \quad b = \frac{\sin(\pi/3-\beta)}{\sin(\pi/3+\alpha)} \quad c = \frac{\sin(\pi/3-\gamma)}{\sin(\pi/3+\beta)}$$

$$e = \left[1+\frac{\sin(\pi/3-\alpha)}{\sin(\pi/3+\gamma)} - \frac{R}{r}\left[\frac{\sin(2\pi/3-\alpha+\gamma)}{\sin(\pi/3+\gamma)}\right]\right]$$

$$f = \left[1+\frac{\sin(\pi/3-\beta)}{\sin(\pi/3+\alpha)} - \frac{R}{r}\left[\frac{\sin(2\pi/3+\alpha-\beta)}{\sin(\pi/3+\alpha)}\right]\right]$$

$$g = \left[1+\frac{\sin(\pi/3-\gamma)}{\sin(\pi/3+\beta)} - \frac{R}{r}\left[\frac{\sin(2\pi/3+\beta-\gamma)}{\sin(\pi/3+\beta)}\right]\right] \quad \text{(A16)}$$

This system has the solution

$$x = \boldsymbol{A}^{-1}\boldsymbol{d}$$

where

$$A^{-1} = \frac{adj(A)}{\det(A)} = \frac{1}{abc+1}\begin{bmatrix} bc & -1 & -b \\ a & ac & -1 \\ 1 & a & ab \end{bmatrix} \quad \text{(A17)}$$

The solution for the three deflections is therefore obtained as

$$\begin{Bmatrix} \delta_\alpha \\ \delta_\beta \\ \delta_\gamma \end{Bmatrix} = \frac{\delta_0}{abc+1}\begin{bmatrix} bc & -1 & -b \\ a & ac & -1 \\ 1 & a & ab \end{bmatrix}\begin{Bmatrix} e \\ f \\ g \end{Bmatrix} \quad \text{(A18)}$$

or

$$\delta_\alpha = \delta_0\frac{ebc+f-gb}{abc+1} \qquad \delta_\beta = \delta_0\frac{acf+g-ce}{abc+1}$$
$$\delta_\gamma = \delta_0\frac{abg+e-af}{abc+1} \quad \text{(A19)}$$

These expressions can be substituted into Equations A7 to A9 to obtain the crack rotation angles.